ingegneria sismica
International Journal of Earthquake Engineering
Anno XLIII - Num. 1 - 2026

Optimization of lightweight design and anti-interference capability of handheld XRF instrument in ore exploration

Jun Xie[1], *Fenfen Sun*[2], *Qingzhu Liu*[2], *Tingting Zhang*[2], *Dong Sui*[2] *and Lin Yang*[1,*]

[1] Cores and Samples Center of Natural Resources CGS, Beijing, 100085, China
[2] CMGB Bu-1 (Hebei) Analysis & Technology Co., Ltd., Langfang, Hebei, 065201, China

SUMMARY: *Handheld X-ray fluorescence spectrometers have been widely used in the detection of elemental content in ore exploration. In this study, a miniaturized tube-excited X-ray fluorescence measurement instrument was designed to meet the lightweight needs of instruments for ore exploration. On this basis, the wavelet denoising algorithm and polynomial fitting method are used to optimize the XRF meter spectra in order to enhance its anti-interference ability. The XRF instrument was applied to detect the heavy metal elements in the ore, and it was found that the optimized XRF instrument spectrum obtained good denoising effect, which effectively smoothed the spectrum and reduced the background interference, and the coefficient of determination of the instrument was improved to 0.9598-0.9972, which indicated that the linear relationship between the content of each heavy metal element in the ore samples and the intensity of the characteristic peaks of X-ray fluorescence spectra was good. Meanwhile, it is verified that the optimized instrument has good precision and correctness, the relative standard deviation is enhanced to 1.17%~4.29%, and the relative error is reduced to 0.21%~2.43%, which can be applied in the field rapid screening of practical ore exploration.*

KEYWORDS: *handheld XRF meter; wavelet denoising; polynomial fitting method; anti-interference ability; ore exploration*

1 Introduction

In the social context of energy crisis, ore exploration can search for deposits with mining value and find out the distribution of mineral deposits, which is of great significance to alleviate the energy crisis and improve the effectiveness of the utilization of natural resources [1, 2]. In the traditional exploration methods, the main methods for ore exploration such as electromagnetic induction method, metal guidance method, gradient measurement method, infrared laser detection method [3, 4]. These methods are mainly through the analysis of gradient information distributed in the ore, the use of active electromagnetic way to achieve the rock and soil layers in the ore detection, in the ore exploration, due to the analog device is bulky and subject to the temperature and humidity and other environmental factors, to complete some complex mathematical operations, the anti-interference performance of the ore detection is not good. The handheld X-ray fluorescence spectrometer (XRF) has been increasingly used in ore exploration in recent years because of its ability to detect elemental content quickly and non-destructively.

Handheld XRF instrument is a kind of analyzer for rapid detection of heavy metals, which has been widely studied and applied in rapid testing of heavy metals in soil samples because of its advantages of simple or no sample pretreatment, fast detection speed and non-destructive

*swzxcsfxs@163.com
https://doi.org/10.65102/is2026069
Published: 30 April, 2026

samples [5-7]. The excitation source of the handheld XRF instrument is mainly a small X-ray tube, which consumes very low energy, so it can be powered by lithium batteries, and generally a lithium battery can work continuously for 4h, and charging is extremely convenient [8, 9]. As it is equipped with a powerful pocket X-ray tube, Si-PIN detector or advanced silicon drift detector, special filters and multi-beam optimization, the analytical performance of XRF can be played to the extreme, making X-ray fluorescence spectrometry can be applied to the detection and analysis in the field [10]. In addition, the handheld XRF instrument is smaller and faster to analyze, and because the XRF analyzer is rugged and portable, it has extremely fast detection speed and accurate detection results, and in the field inspection, it almost does not rely on the laboratory test far away from the detection environment, and instantly makes the analysis results [11, 12]. Based on these advantages, the application of handheld XRF instruments in ore exploration can meet the needs of lightweight design and optimization of anti-interference capability.

Regarding the application of handheld XRF instruments and their related technologies in ore exploration, detection and analysis and their advantages, the literature [13] evaluated the application and advantages of handheld XRF instruments in the exploration of special metals, examined the detection accuracy and applicable concentration range of rare earths, niobium, and other elements by analyzing the data of multiple standards, and emphasized its rapid decision-making in the field of carbonate rock-related deposits. It also emphasizes its practical value in the rapid decision-making in the field of carbonatite-related deposits, and at the same time points out its technical limitations in the detection of low concentration and other aspects. Literature [14] proposed and validated a method for analyzing the chemical composition of carbonate veins using a handheld XRF instrument, examined its potential application in identifying multigenerational carbonate-filled veins by developing a quality assurance process and calibration equations based on certified reference materials, and highlighted the significant advantages of the method in providing a basis for critical decision-making in mineral exploration in a rapid and cost-effective manner. Literature [15] analyzed drill hole samples from the Xigangzhisu porphyry copper deposit using a handheld XRF instrument, investigated its deep mineralization potential through primary halo element zoning sequences and ratio characteristics, pointed out the possibility of the existence of a concealed ore body, and emphasized the technique's outstanding advantages in rapid, efficient, and environmentally friendly on-site geochemical assessment. Literature [16] analyzed the performance of high-density measurements of multiple principal trace elements in marine core samples by developing a shipboard quantitative analysis solution for a handheld XRF instrument, pointed out that the measurement results were highly consistent with shipboard ICP-OES within the error range, and emphasized that the technology can identify the chemical stratigraphy in real time, optimize sampling and drilling decisions, and greatly enhance the exploration efficiency and data value.

Literature [17] analyzed the application of handheld XRF instrument in the field analysis of cobalt-rich crusts, established the calibration curve through the standard material, verified the advantages of its rapid and non-destructive measurement, and emphasized the high consistency between the method and the laboratory results, which can satisfy the dual needs of rapid resource assessment and metallogenic research in marine exploration. Literature [18] ta discusses the application advantages of handheld XRF instrument in ore exploration for rapid and economic acquisition of field data, and at the same time investigates the key factors affecting the interpretation of its measurement results, emphasizing the importance of understanding the depth of excitation volume and the detection limit for avoiding misinterpretation of the data, with the aim of providing practical guidance for non-professional users. Literature [19] validated a workflow for rapid acquisition of stable handheld XRF data

in weathered crust exploration environments, analyzed the advantages of its accuracy for Cu, Zn, Fe and other elemental measurements by comparing with laboratory data, and emphasized its ability to support on-site real-time drilling decision-making to greatly enhance exploration efficiency and economy. Literature [20] analyzed the advantages of handheld XRF instrument in mineral exploration, through comparison and verification, pointed out that it can quickly obtain multi-element data without pre-processing and good correlation with the laboratory results, and emphasized that the technology is suitable for semi-quantitative trend analysis and assisted decision-making, but can not completely replace the traditional whole-rock geochemistry methods.

Literature [21] addressed the calcium spectral interference faced by handheld XRF instrument when analyzing scandium in nickel laterite, and by comparing the three quantitative methods, pointed out that the method based on spectral fitting and improved experimental conditions can effectively expand the reliable measurement range and reduce the error, and emphasized the key role of optimizing the interference management to improve the reliability of field analysis. Literature [22] used a handheld XRF instrument to analyze elemental concentrations in ores and associated plant specimens, and solved the inherent limitation of the equipment to quantify inaccuracies in thin samples by developing an independent data processing flow, thus enhancing the overall reliability of elemental field analysis in ore exploration. Literature [23] examined the application of a handheld XRF instrument in the early exploration of gold ores, pointed out the need to calibrate laboratory whole-rock analyses as a reference when prefabricated standards are insufficient, investigated the problem of underestimation of concentrations due to paper-bagged samples, and emphasized that consideration of data quality and calibration is essential to ensure analytical accuracy. Literature [24] examined the application of handheld XRF instruments in the exploration of carbonate-type sulfide deposits in the Otavi Mountains, and analyzed the good detection accuracy and correlation of major elements such as Cu, Pb, and Zn by comparing laboratory methods such as ICP-MS, and pointed out the limitations in the analysis of trace elements such as silver, and emphasized the applicability and economic advantages of this technology as a low-cost and efficient field tool. The advantages of this technique are also emphasized as a low-cost and efficient field tool. Literature [25] analyzed the application of handheld XRF instrument in porphyry copper exploration, and by comparing its estimation of whole rock composition with that of optical mineralogy, pointed out that there are systematic deviations in the judgment of sulfur, copper and other elements, and discussed the potential influence of vein structure on the measurements, which emphasized the applicability and inherent limitations of this technology in rapid on-site judgment. Literature [26] studied the application of handheld XRF instrument in the exploration of hydrothermal sulfide sediments in the Southwest Indian Ridge. By comparing sediment samples with different grain sizes and distances from vents, it pointed out its efficient identification ability of mineralized elements such as Cu, Zn, Fe, etc., and emphasized the key law of sediment grain size and elemental partitioning, which confirms that this technique can meet the needs of rapid identification of seafloor geochemical anomalies. Literature [27] explored the application of a handheld XRF instrument for the determination of metal content in iron ore concentrates, which significantly improved the accuracy of iron element analysis through linear calibration, and emphasized its great potential for rapid, non-destructive multi-element quantitative analysis in the smelting industry. Literature [28] presents a model that combines a handheld XRF meter with XRD analysis to determine the mineral composition of rocks, improves the reliability of its chemical composition analysis through calibration, and emphasizes the advantages of this method for rapid and economical drill cuttings and archival core applications.

The study is to carry out a lightweight design of the handheld XRF instrument, which adopts

a small X-ray tube, a small Si-PIN semiconductor detector and a pocket-sized computer as the building blocks, and reduces the size of the XRF instrument to a large extent. Aiming at the problem that the fluorescence spectrum of XRF instrument is easily interfered by noise, the wavelet transform algorithm is used to denoise the signal, and the polynomial fitting method based on maximum filtering is proposed to realize the automatic deduction of background and improve the spectral quality, so as to optimize the anti-interference ability of the XRF instrument. Ore samples are selected for experiments to compare the spectra before and after optimization, the spectral background fitting diagrams, and the coefficients of determination of the standard curves, to determine the optimization effect of the proposed algorithm, and then examine the method detection limit, precision, and correctness, to analyze the feasibility of the application of the XRF method to the determination of various elements in the exploration of ores.

2 Lightweight design for handheld XRF meters

2.1 Instrument structure

X-ray fluorescence analysis (XRF) is a method of analyzing the composition of substances and studying chemical states by using primary X-ray photons or other microscopic particles to excite the atoms in the substances to be measured, causing them to produce fluorescence (secondary X-rays).

In order to meet the needs of ore exploration, the lightweight design study is mainly carried out for these elements, and the following key technologies are adopted: (1) a controllable X-ray source composed of a low-power compact X-ray tube and a high-voltage power supply, (2) a small, low-power electrocooled Si-PIN semiconductor detector with high energy resolution as the detecting element, and (3) a pocket computer as the working platform to form an X-ray fluorescence spectroscopy analysis system, according to the requirements of the working environment, in the resident can directly use (laptop) microcomputer to realize microcomputerization, use its powerful functions, in the field using Pocket PC, to achieve the instrument's portability and in-situ measurement. The structural block diagram of the miniaturized tube-excited X-ray fluorescence measurement instrument is shown in Fig. 1, which is mainly composed of a controllable X-ray excitation source, semiconductor detector, main amplifier, power supply, multi-channel pulse amplitude analyzer (MCA), Pocket PC and (laptop) microcomputer system.

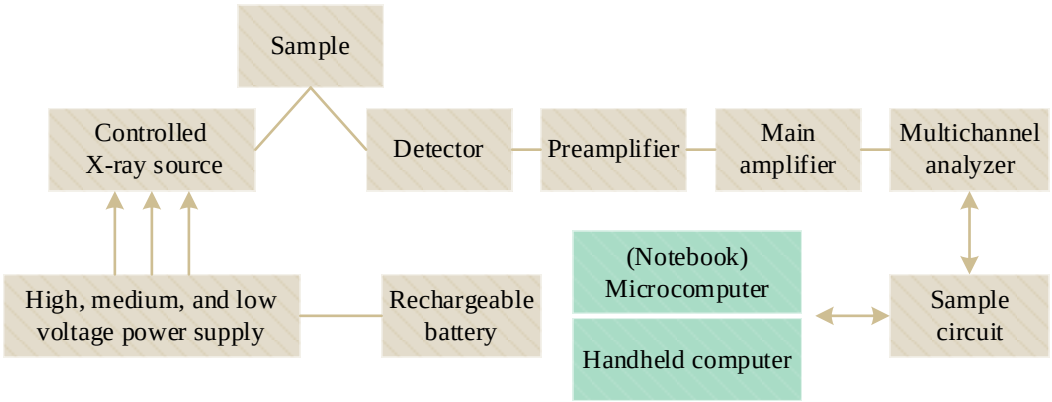

Figure 1: structure of the XRF instrument with X-ray tube

2.2 System components

2.2.1 Controlled X-ray excitation sources

The controlled X-ray excitation source consists of a small, low-power X-ray tube and a high-voltage power supply for X-ray tube operation.

(1) By adjusting the high voltage, the X-ray output energy of the controllable X-ray source is adjustable (continuously adjustable within the range of 5 to 35 keV), which facilitates the task of multi-element determination.

(2) By adjusting the gate voltage and changing the beam current intensity of the X-ray source, it can provide excitation rays with high irradiation rate, thus effectively improving the detection limit of the on-site X-ray fluorescence instrument and raising the level of analysis.

(3) No radiation pollution to the workplace environment.

(4) The power of the controllable X-ray source is 4W, and the stability of the output energy and beam current intensity is good.

2.2.2 X-ray detectors

A small, low-power electrocooled Si-PIN semiconductor detector with high energy resolution is used as the detection element. It maintains the features of good energy resolution and wide energy linear range of general semiconductor detectors. The external dimensions are 7cm×5cm×3cm, the weight is about 500g, and the power consumption of the electrocooling source is 1W, which is a more ideal detection element for on-site miniaturized tube-excited X-ray fluorescence instrument.

2.2.3 Microcomputerization and interfaces

Pocket PCs and laptop microcomputers are used to realize microcomputerization. With low power consumption, small size, light weight and strong functions, the Pocket PC can realize automatic acquisition of field spectral data, spectral line display and X-ray fluorescence spectral analysis, directly calculate elemental content, and easily exchange data with the microcomputer, thus completing further mapping and outputting of survey area results. As a result of the use of notebooks and palmtop computers to realize microcomputerization, the serial interface communication mode.

3 Experimental section

3.1 Instruments and main reagents

The handheld XRF instrument in this paper was selected as a miniaturized tube-excited X-ray fluorescence measurement instrument with lightweight design.

H_3BO_3: blank control to determine the detection limit of the instrument. National standard ore samples (purchased from the National Research Center for National Standards): to determine the accuracy and precision of the instrument. Actual ore samples: to establish the standard curve and verify its accuracy. Vinyl sample cup: 30 mm in diameter x 10 mm in height, with a neck ring for fixing the Mylar film. Mylar film: special film for X-ray analysis, 6μm thick. Ball mill: used in the process of sample preparation.

Ore composition analysis standard substances: GBW07103~GBW07106, GBW07120~ GBW7122.

3.2 Experimental Methods

3.2.1 Sample preparation

The actual ore samples collected from a site were naturally air-dried to remove obvious foreign materials such as grass clippings and animal fragments from the ore samples, and two portions were taken using the tetrad method, one for experimental analysis and one for retention and reserve. The ore standard samples and the experimentally analyzed ore samples were uniformly filled into the agate mantle, and the powder was removed and sieved through a 200 mesh (74 μm) sieve after grinding for 5 min on a ball mill.

The sieved sample was filled into the sample cup, dried and then compacted with a presser, and the ore samples were sealed with Mylar film to ensure that the samples would not leak out, and then the probe window of the instrument was aligned with the ore samples, and there should not be a gap between the samples and the probe to ensure the accuracy of the test results.

3.2.2 Standard curve establishment

Load the treated soil samples, fix the Mylar film on the vinyl sample cup, press it tightly, and test the ore samples with this miniaturized tube-excited X-ray fluorescence spectrometer, and measure each sample five times. The respective counts of copper, chromium, zinc, nickel, arsenic and lead were averaged and a standard curve was established with their corresponding standard values (national standard samples). Because the heavy metal elements in the ore are greatly affected by the superposition of coexisting elements, absorption-enhancement effect, signal noise and matrix interference, the direct establishment of the standard curve linearity will be poor, so before the detection of the samples, it is necessary to instrumental measurement of the spectrum of the noise reduction, background deduction and other processing before the linear regression, and finally the establishment of the optimized standard curve.

3.2.3 Validation of standard curves

After the standard curve was established, the measured spectra were re-tuned into the software to obtain the detected values of the ore samples, and the detected values were compared with the standard values and calculated. Due to the experiments measured more soil samples, in order to more intuitively reflect the accuracy of the detection results, selected samples with different heavy metal content of the ore and H_3BO_3 (blank control) for scanning detection, and each sample was scanned five times after the processing, to examine the stability and accuracy of the instrument.

3.2.4 Data processing

Data were statistically analyzed using Excel 2010, SPSS 19.0 and MatlabR2012a software.

3.3 Anti-jamming capability optimization method

The fluorescence spectrum measured by the X-ray fluorescence spectrometer generally contains noise under the combined effect of the statistical rise and fall of the detector, the noise of the electronic components, the interference of the surrounding environment, and the perturbation of the experimental conditions. Noise affects the accuracy of background deduction, so that there is a loss of weak peaks in the detection of characteristic peaks, finding false peaks, and an increase in the deviation of the net peak area. Therefore, the noise in the spectrum is filtered out before further processing of the spectrum to improve the anti-interference ability of the instrument and analysis accuracy. In this paper, wavelet denoising

algorithm realizes smooth denoising of the signal and removes the spectral baseline using polynomial fitting method.

3.3.1 Wavelet Denoising Algorithm

The wavelet change was developed from the Fourier transform, which was introduced so that signals in the time domain could be converted to signals in the frequency domain with the formula:

$$X(j\omega) = \int_{-\infty}^{\infty} x(t) e^{-j\omega t} dt \tag{1}$$

$$x(t) = \frac{1}{2\pi} \int_{-\infty}^{\infty} X(j\omega) e^{j\omega t} d\omega \tag{2}$$

However, for non-smooth signals, the Fourier transform does not perform very well, which led to the emergence of an improved Fourier transform - the short-time Fourier transform. This is the Fourier transform of the original signal multiplied by the window function, which divides the non-smooth signal into small segments, each segment can be regarded as a sequence of smooth signals, and the Fourier transform is performed on each small segment, which is expressed as:

$$STFTx(w)(t', f) = \int \left[x(t) * w^{*t-t'} \right] * e^{-j2\pi ft} dt \tag{3}$$

In order to obtain better time-frequency resolution, wavelet techniques that can represent signals in both time and frequency domains have been proposed to be able to store information better. The wavelet transform is categorized into continuous wavelet transform and discrete wavelet transform, which are represented by the formulas as (4) and (5), respectively:

$$CWT(a,b; x(t), \psi(t)) = \int_{-\infty}^{\infty} \left[x(t) \cdot \frac{1}{a} \cdot \psi^* \left(\frac{t-b}{a} \right) \right] dt \tag{4}$$

$$DWT\left[n, a^j \right] = \sum_{m=0}^{N-1} x[m] \cdot \psi^*{}_j \left[m-n \right], \psi_j[n] = \frac{1}{\sqrt{a^j}} \psi \left(\frac{n}{a^j} \right) \tag{5}$$

In Eq. (4) $x(t)$ is the original signal sequence, $\psi(t)$ is the mother wavelet, i.e., the analyzing function, a is the scale parameter, and b denotes the time position. The similarity between the two functions is measured by using the inner product of the mother wavelet and the original signal and integrating it, and varying the time parameter (a) to compress or stretch the mother wavelet, and varying the position parameter (b) to obtain the frequency information at different positions. In Eq. (5) n is the delay parameter, N is the signal length, and ψ is the discrete mother wavelet function.

The use of wavelet transform for denoising is due to the fact that the energy of the signal containing useful information is mainly concentrated in some large wavelet coefficients in the wavelet domain, while the energy of the noise is distributed throughout the wavelet domain. Therefore, after wavelet decomposition, the amplitude of the wavelet coefficients that contain useful information signals is larger than the amplitude of the coefficients of noise, that is, it can be assumed that the wavelet coefficients with larger amplitudes are generally dominated by

signals that contain useful information, while the coefficients with smaller amplitudes are to a large extent noise. Thus, a thresholding approach is used to attenuate most of the noise coefficients to 0, i.e., coefficients smaller than the thresholded portion are removed as interfering noise, and then wavelet reconstruction is performed to achieve noise reduction.

For a given threshold, there are generally two types of denoising processes, namely, soft thresholding and hard thresholding. The formula for soft thresholding is expressed as:

$$w_\lambda = \begin{cases} \operatorname{sgn}(w)\cdot(|w|-\lambda) & |w| \geq \lambda \\ 0 & |w| \leq \lambda \end{cases} \tag{6}$$

The formula for the hard threshold is expressed as:

$$w_\lambda = \begin{cases} w, & |w| \geq \lambda \\ 0, & |w| < \lambda \end{cases} \tag{7}$$

And there are many ways to determine the threshold, in this paper we use the unbiased risk estimation threshold, fixed threshold, very large and very small thresholds which are often used in wavelet denoising, for the signal sequence $\{S(i), i = 1, 2, \cdots\cdots, N\}$ whose length is N, its determination of thresholds is are as follows:

(1) Threshold for unbiased risk estimation: Sort its absolute values from smallest to largest, noting the k th value after sorting as $sort_k(|S|)$, squaring it to obtain $f(k) = (sort_k(|S|))^2$, and then calculating the risk vector $Risk$, with the k th element having the value of $Risk_k = \dfrac{N - 2k + \sum_{i=1}^{k} f(i) + (N-k)\cdot f(N-k)}{N}$, then the point $k_{\min}$ with the smallest risk value in the risk vector is the unbiased risk threshold estimate:

$$\lambda_k = \sqrt{f(k_{\min})} \tag{8}$$

(2) Fixed thresholds:

$$\lambda = \sqrt{2 \cdot \log N} \tag{9}$$

(3) Extremely large and very small thresholds:

$$\lambda = \begin{cases} 0.3936 + 0.1829 \cdot \dfrac{\ln N}{\ln 2}, & N \geq 32 \\ 0, & N \leq 32 \end{cases} \tag{10}$$

(4) Heuristic thresholding

The values of $crit$ and eta are calculated separately, and if $crit < eta$, a fixed threshold is used for the threshold. If $crit \geq eta$, the threshold is selected as the smaller of the fixed threshold and the unbiased risk estimation threshold. Where the value of $crit$ is:

$$crit = \sqrt{\frac{\left(\log_2 N\right)^3}{N}} \tag{11}$$

The value of eta is:

$$eta = \frac{\sum_{j=1}^{N}\left(\left|S_j\right| - N\right)}{N} \tag{12}$$

For the signal sequence, the signal-to-noise ratio, mean square error and information entropy are used as evaluation indexes of denoising effect. For the original signal sequence $f(k), k = 1, 2, \cdots, N$ of length N and the sequence after noise reduction is $\hat{f}(k), k = 1, 2, \cdots, N$, the signal-to-noise ratio is computed:

$$SNR = 10\log \frac{\sum_{n=1}^{N} f(n)^2}{\sum_{n=1}^{N}\left[f(n) - f(\hat{n})\right]^2} \tag{13}$$

The formula for calculating the mean square error:

$$MSE = \frac{\sum_{n=1}^{N}\left[f(n) - f(\hat{n})\right]^2}{N} \tag{14}$$

The information entropy is calculated as:

$$H = -\sum_{i=1}^{N} p(x_i)\log_2 p(x_i) \tag{15}$$

where N denotes the number of channels of the spectral line, $f(n)$ denotes the original signal, $f(\hat{n})$ denotes the processed estimated signal, and $p(x_i)$ denotes the probability of the information appearing at the point.

In order to comprehensively evaluate the denoising effect, the coefficient α (which is inversely proportional to the denoising effect) is established with the formula:

$$\alpha = \frac{MSE}{SNR \times H} \tag{16}$$

3.3.2 Polynomial fitting method

The main background in the fluorescence spectra obtained with an X-ray tube as the excitation source is the continuous X-ray spectrum, which is a more slowly varying curve. The polynomial fitting method is used to polynomially fit the background in the background region, and the polynomial parameters are obtained by the least squares method, and then interpolated to obtain the background in the peak region. When the polynomial number is chosen too small, the background region will be underfitted and the overall fitting effect is poor. This paper proposes the polynomial fitting method based on maximum filtering (MFPFM) on its basis, which adopts the iterative idea to gradually remove the data in the peak area, and uses the number of points whose fitting result is less than 0 to judge whether the polynomial number is appropriate or

not.The steps of MFPFM are as follows:

(1) Set the boundary threshold t_e, search the first count value larger than t_e from left to right on the spectrum $x(i)$, and take its channel address as the starting channel address $start$ for the fitting. Search the spectrum $x(i)$ from right to left for the first count value larger than t_e, and use its address as the e end of the fit.

(2) Construct the channel address vector $c(j)$ and the spectral vector $y(j)$ with the following equations:

$$\begin{cases} c(j) = j \\ y(j) = x\left(start + j\right) \end{cases} \left(j = 0,1,\cdots,J\right) \tag{17}$$

where $J = end - start + 1$, denotes the number of points in $y(j)$.

(3) Do polynomial fitting on $c(j)$ and $y(j)$ to obtain the fitting result $p(j)$:

$$p(j) = \sum_{m=0}^{k} a_m c^m(j) \left(j = 0,1,\cdots,J-1\right) \tag{18}$$

where k is the polynomial number and a_m is the polynomial coefficient.

(4) Compute the standard deviation σ of the estimated background $q(j) = y(j) - p(j)$, and $q(j)$.

(5) Determine whether the maximum value in $q(j)$ is less than 2σ:

$$\max\left(q(j)\right) < 2\sigma \tag{19}$$

If it is less than then delete the channel address and count value corresponding to the maximum value from $c(j)$ and $y(j)$ respectively, $J = J - 1$, and then continue to execute (3), otherwise execute (6).

(6) $p(j)$ is the background region background, use equation (18) to calculate the value when $j = \left(0,1,\cdots,J-1\right)$ to obtain the complete estimated background $r(j)$.

(7) Set the zero threshold t_z and the maximum number of times K, if the number of points n_z less than 0 in $r(j)$ is greater than t_z and the polynomial number of times k is less than K, then make $k = k + 1$, and execute (2), otherwise, it means that k is of appropriate size, and execute (8).

(8) To prevent the fitting background $r(j)$ from being too large, take the minimum of $r(j)$ and $x(j + start)$ as the corrected background $s(j)$.

(9) The count values to the left of $start$ and the count values to the right of end are used as the background, and $s(j)$ are combined to form the estimated background $u(i)$ of the original spectrum $x(i)$:

$$u(i) = \begin{cases} s(i - start) & start \le i \le end \\ x(i) & others \end{cases} \tag{20}$$

4 Results and discussion

4.1 Anti-jamming optimization effect

4.1.1 Selection of wavelet bases

To carry out the wavelet transform, first of all, we need to choose the appropriate wavelet base, symmetry, orthogonality, tight support and support width, etc. Different will produce different denoising effect, experiments using Matlab on the spectral line smooth denoising processing, select some commonly used wavelet base, fixed wavelet decomposition layer number and threshold, and then change the wavelet base running results. In order to ensure the consistency between the denoised spectrum and the original spectrum, three indexes, namely, signal-to-noise ratio (SNR), root-mean-square error (MSE) and information entropy (H), are chosen to evaluate the denoising effect. Among them, the larger the SNR, the better the H, and the smaller the MSE, the better. The coefficient α is the combined denoising effect of the three indicators, the smaller the better.

The denoising effect of different wavelets is evaluated as shown in Table 1. When Coif4 wavelet base is selected, α is minimized, and experiments are conducted on the number of decomposition layers, and when the number of decomposition layers = 4, α is minimized to 36.86, so Coif4 wavelet base is finally selected for four-layer decomposition.

Table 1: Denoising effects evaluation of different wavelets

	SNR	MSE	H	α
Coif4	109.64	518.89	0.122	36.86
Coif5	109.12	518.21	0.118	38.21
Db7	99.84	523.11	0.121	41.63
Db9	110.27	517.66	0.119	37.56
Sym6	104.48	519.93	0.112	42.37
Sym7	106.95	518.54	0.108	42.61

4.1.2 Smoothing effects on spectral lines

Taking GBW07103 ore sample spectral line processing as an example, Fig. 2 shows the spectral line smoothing denoising effect comparison diagram and its local enlargement, in which the horizontal coordinate represents the energy value, the vertical coordinate represents the count rate, Fig. (a) is the original spectrum, and Fig. (b) is the denoised spectrum. From the figure, it can be seen that the use of wavelet denoising method effectively removes the interference of noise and achieves the smoothing of the spectral line, indicating that the use of wavelet threshold filtering can effectively smooth the spectral line, fitting false peaks and noise signals, which is conducive to the optimization of X-ray fluorescence measurement of the anti-jamming ability of the instrument.

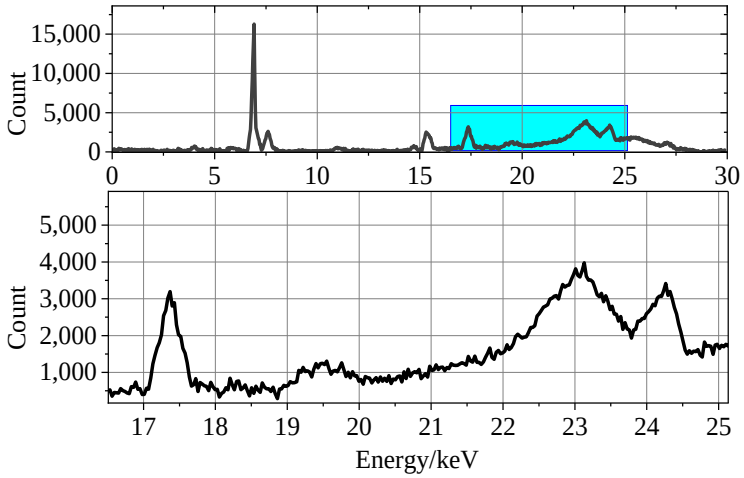

(a)Original signal and partial enlarged view

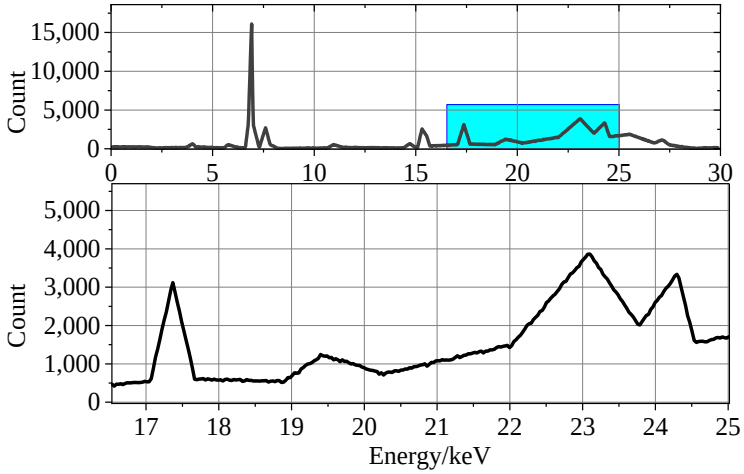

(b)Denoised signal and partial enlarged view

Figure 2: Wavelet transform processing results

4.1.3 Spectral line processing

The polynomial fitting method based on maximum filtering was utilized to process the spectra of GBW07103 ore samples, and Fig. 3 shows the spectral background fitting plot and its local enlargement, and Fig. 4 shows the comparison between before and after the spectral background deduction, where the horizontal coordinates represent the number of channels, and the vertical coordinates represent the intensity counts. The wavelet transform and iterative polynomial fitting are utilized to effectively remove the noise interference and background deduction, and the experiment is basically stabilized by the fitted baseline after 8 iterations. The spectral lines are processed to effectively smooth the spectral lines and reduce the background interference, fitting false peaks and noise signals, thus facilitating the quantitative analysis of the energy spectrum.

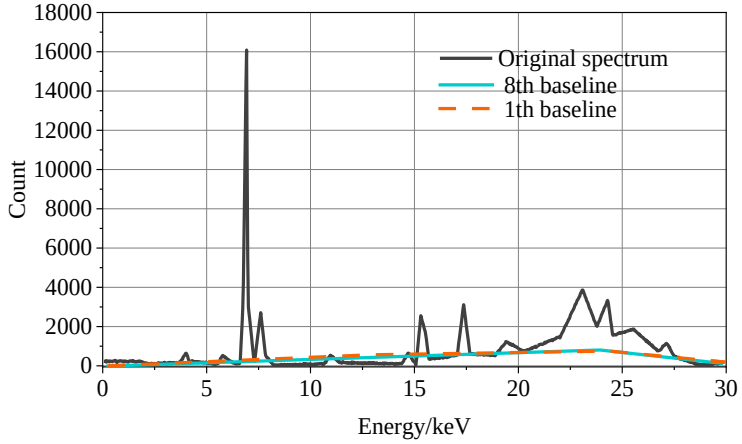

Figure 3: Background baseline for GBW07103 ore standard sample

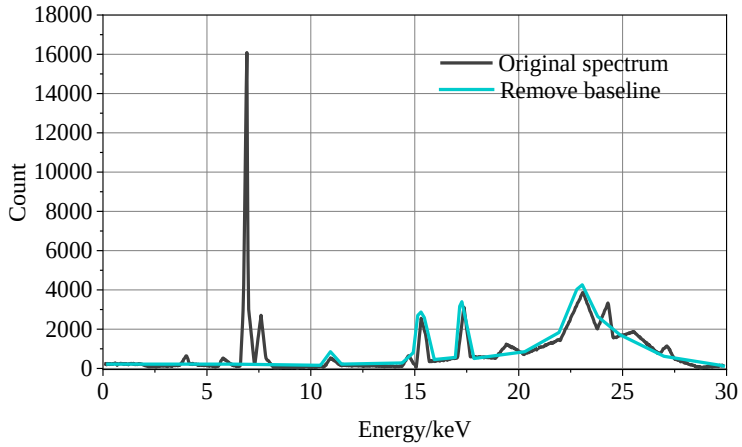

Figure 4: Background deduction results for GBW07103 ore standard sample

4.1.4 Plotting of standard curves

The processed spectral line values were used to draw the standard curve, and the coefficients of determination before and after the optimization of the algorithm are shown in Table 2. After the processing of noise reduction and background deduction, the R2 of the standard curves obtained was improved to 0.9598-0.9972, especially for Ni, and compared with that before the processing, the R2 was improved from 0.7629 to 0.9885, which indicated that after the processing of noise reduction and background deduction, the standard curve fit of some elements was better and more convenient for the quantitative analysis. This indicates that after the noise reduction and background deduction treatment, the standard curve fitting effect of some elements is better, which is more conducive to quantitative analysis, and the anti-interference and accuracy of the data are also improved. The linear relationship between the content of each heavy metal element in the ore and the intensity of X-ray fluorescence spectra is good, and the model is established, which can be used as the standard curve of the instrument.

Table 2: Determination coefficients before and after optimization

Element	Content range/%	R^2	
		Before optimization	After optimization
Ni	0.023~3.49	0.7629	0.9885
Pb	0.010~26.9	0.9347	0.9613
Cu	0.028~12.3	0.9866	0.9925
As	0.017~6.06	0.9456	0.9598
Zn	0.19~26.0	0.9916	0.9972
Cr	0.037~10.9	0.9587	0.9687

4.2 Limit of detection of the method

The limit of detection (LOD) of a method is an important index for evaluating an analytical method, which refers to the smallest concentration of the analyte to be analyzed that can be detected within a given level of significance by a given analytical method (including sample pretreatment). The XRF method was optimized using wavelet denoising and polynomial fitting for 20 consecutive determinations of the rock specimen GBW07105, and the detection limits were calculated as the concentrations corresponding to three times the standard deviation, and Table 3 shows the average values of the detection limits of heavy metal elements in the ore specimen GBW07105. The detection limits of Ni, Pb, Cu, As, Zn and Cr in the ore were 5.07 μg/g, 11.52 μg/g, 7.38 μg/g, 7.11 μg/g, 3.52 μg/g and 21.95 μg/g, respectively.

Table 3: Detection limit of each element

Element	Detection limit(μg/g)
Ni	5.07
Pb	11.52
Cu	7.38
As	7.11
Zn	3.52
Cr	21.95

4.3 Precision of the method

The ore specimen GBW07105 was selected to repeatedly prepare five presses, and the precision results of the ore specimen were measured on the five samples, as shown in Table 4. The relative standard deviations (RSDs) of the determination results of various heavy metal elements for the ore samples were 2.56%~6.00% before optimization and 1.17%~4.29% after optimization, and the detection precision of the XRF method was higher after optimization using wavelet denoising and polynomial fitting.

Table 4: Precision results of ore sample

Element	Standard value(μg/g)	Found(μg/g)		RSD/%	
		Before optimization	After optimization	Before optimization	After optimization
Ni	140	146.41	142.35	4.58%	1.68%
Pb	7	6.58	6.74	6.00%	3.71%
Cu	49	46.84	50.35	4.41%	2.76%
As	0.70	0.74	0.67	5.71%	4.29%
Zn	150	155.49	152.29	3.66%	1.53%
Cr	134	130.57	132.43	2.56%	1.17%

4.4 Correctness of methodology

The correctness of this method was verified by the ore specimen GBW07107, and the experimental results of the correctness are shown in Table 5. The relative errors of the determination of various heavy metal elements of the ore specimen were 0.36%~4.10% before the optimization of the XRF method, and 0.21%~2.43% after the optimization, and the correctness was better after the optimization on the whole.

Table 5: Trueness results for ore sample

Element	Certified (μg/g)	Found(μg/g)		Relative error/%	
		Before optimization	After optimization	Before optimization	After optimization
Ni	37±4	35.76	37.81	3.35%	2.19%
Pb	8.7±2.7	8.48	8.56	2.53%	1.61%
Cu	21±2	21.59	20.73	2.81%	1.29%
As	1.4±0.4	1.405	1.403	0.36%	0.21%
Zn	58±6	55.62	59.41	4.10%	2.43%
Cr	31±5	31.96	30.52	3.10%	1.55%

5 Conclusion

In this paper, the handheld XRF instrument is designed to be lightweight, combined with wavelet denoising and polynomial fitting methods to denoise and remove the spectral baseline of the XRF instrument in order to enhance the anti-interference ability of the XRF instrument, and to conduct experimental analysis of the detection of heavy metal elements in ores. The main research results are as follows:

(1) The XRF instrument adopts a small X-ray tube as the controllable X-ray source, a small Si-PIN semiconductor detector as the X-ray detector, and a Pocket PC and a laptop microcomputer as the working platform to realize the light weight of the handheld XRF instrument.

(2) The Coif4 wavelet basis is selected for denoising and the polynomial fitting method based on maximum filtering is utilized to deal with the spectral background, which achieves an obvious spectral smooth denoising effect and improves the anti-interference ability of the XRF instrument. Compared with the original spectra, the determination coefficients of the standard curves were enhanced to 0.9598-0.9972, which improved the quantitative analysis capability of the XRF instrument.

(3) The optimized XRF instrument can detect the content of heavy metals in the ore, the detection limit of the instrument is loaded to the standard value, and the relative standard deviation of the XRF method for the detection of all kinds of elements in the ore is improved from 2.56%~6.00% before the optimization to 1.17%~4.29% after the optimization, and the relative error is reduced from 0.36%~4.10% to 0.21%~2.43% before the optimization, showing a higher precision. The relative error is reduced from 0.36%~4.10% before optimization to 0.21%~2.43%, which shows higher precision and correctness.

About the Author

Jun Xie was born in Tangshan, Hebei. China, in 1982. He obtained a bachelor's degree from China University of Geosciences (Beijing). He currently working at Cores and Samples Center

of Natural Resources CGS. His main research direction is geology experiment testing.

Lin Yang was born in Tongchan, Shaanxi. China, in 1983. He obtained a bachelor's degree from Changchun Institute Of Technology. He currently working at Cores and Samples Center of Natural Resources CGS. His main research direction is geology experiment testing.

Fenfen Sun was born in Jining, Shandong, China in 1989. She obtained a Master's degree from Chengdu University of Technology. She is currently working at CMGB Bu-1 (Hebei) Analysis & Technology Co., Ltd. Her main research direction is geology experient testing.

Qingzhu Liu was born in Tianzhu Guizhou, China in 1986. She obtained a Master's degree from Chengdu University of Technology. She is currently working at CMGB Bu-1 (Hebei) Analysis & Technology Co., Ltd. Her main research direction is geology experient testing.

Tingting Zhang was born in Lanzhou, Gansu, China in 1990. She obtained a Master's degree from Chengdu University of Technology. She is currently working at CMGB Bu-1 (Hebei) Analysis & Technology Co., Ltd. Her main research direction is Environmental and Geological Testing.

Dong Sui was born in Jixi, Heilongjiang, China, in 1985. He obtained a bachelor's degree from Changchun Institute of Technology. He currently working at CMGB Bu-1 (Hebei) Analysis & Technology Co., Ltd. His main research direction is geology experient testing.

References

[1] Okada, K. (2022). Breakthrough technologies for mineral exploration. Mineral Economics, 35(3-4), 429.

[2] Shirani Faradonbeh, R., Shah, M. I., Bahadori, M., & Jang, H. (2025). Toward Sustainable Mining: Exploring Alternative Mineral Resources and Innovative Extraction Techniques. Mining, 5(4), 66.

[3] Guo, Z., Xue, G., Liu, J., & Wu, X. (2020). Electromagnetic methods for mineral exploration in China: A review. Ore Geology Reviews, 118, 103357.

[4] Okada, K. (2021). A historical overview of the past three decades of mineral exploration technology. Natural Resources Research, 30(4), 2839-2860.

[5] Zhou, S., Wang, J., Wang, W., & Liao, S. (2023). Evaluation of portable X-ray fluorescence analysis and its applicability as a tool in geochemical exploration. Minerals, 13(2), 166.

[6] Bosco, G. L. (2013). Development and application of portable, hand-held X-ray fluorescence spectrometers. TrAC Trends in Analytical Chemistry, 45, 121-134.

[7] Young, K. E., Evans, C. A., Hodges, K. V., Bleacher, J. E., & Graff, T. G. (2016). A review of the handheld X-ray fluorescence spectrometer as a tool for field geologic investigations on Earth and in planetary surface exploration. Applied Geochemistry, 72, 77-87.

[8] Drake, B. L., & MacDonald, B. L. (Eds.). (2022). Advances in portable X-ray Fluorescence spectrometry: instrumentation, application and interpretation. Royal Society of Chemistry.

[9] Barago, N., Pavoni, E., Floreani, F., Crosera, M., Adami, G., Lenaz, D., ... & Covelli, S. (2022). Portable X-ray fluorescence (pXRF) as a tool for environmental characterisation

and management of mining wastes: Benefits and limits. Applied Sciences, 12(23), 12189.

[10] Lemiere, B., & Uvarova, Y. (2017, October). Introduction: New developments in field portable geochemical techniques and site technologies and their place in mineral exploration. In Exploration 17, Field Analysis Workshop.

[11] Vanhoof, C., Bacon, J. R., Fittschen, U. E., & Vincze, L. (2021). Atomic spectrometry update–a review of advances in X-ray fluorescence spectrometry and its special applications. Journal of Analytical Atomic Spectrometry, 36(9), 1797-1812.

[12] Saker-Clark, M., Kemp, D. B., & Coe, A. L. (2019). Portable X-ray fluorescence spectroscopy as a tool for cyclostratigraphy. Geochemistry, Geophysics, Geosystems, 20(5), 2531-2541.

[13] Simandl, G. J., Stone, R. S., Paradis, S., Fajber, R., Reid, H. M., & Grattan, K. (2014). An assessment of a handheld X-ray fluorescence instrument for use in exploration and development with an emphasis on REEs and related specialty metals. Mineralium Deposita, 49(8), 999-1012.

[14] Andrew, B. S., & Barker, S. L. (2018). Determination of carbonate vein chemistry using portable X-ray fluorescence and its application to mineral exploration. Geochemistry: Exploration, Environment, Analysis, 18(1), 85-93.

[15] Li, Z., Wei, N., Li, M., Wu, S., Li, H., & Liu, P. (2025). Application of Portable X-Ray Fluorescence Analysis in Mineral Exploration: A Case Study from Cimabanshuo Porphyry Copper Deposit. Minerals, 15(12), 1286.

[16] Ryan, J. G., Shervais, J. W., Li, Y., Reagan, M. K., Li, H. Y., Heaton, D., ... & IODP Expedition 352 Scientific Team. (2017). Application of a handheld X-ray fluorescence spectrometer for real-time, high-density quantitative analysis of drilled igneous rocks and sediments during IODP Expedition 352. Chemical Geology, 451, 55-66.

[17] ZHANG, X. H., Qiang, L. I., & HUANG, X. H. (2014). Application of Hand-held X-ray Fluorescence Spectrometer in the Exploration of Cobalt-rich Crust Resources. Rock and Mineral Analysis, 33(4), 512-516.

[18] Potts, P. J., & Sargent, M. (2022). In situ measurements using hand-held XRF spectrometers: a tutorial review. Journal of Analytical Atomic Spectrometry, 37(10), 1928-1947.

[19] Gazley, M. F., Bonnett, L. C., Fisher, L. A., Salama, W., & Price, J. H. (2017). A workflow for exploration sampling in regolith-dominated terranes using portable X-ray fluorescence: comparison with laboratory data and a case study. Australian Journal of Earth Sciences, 64(7), 903-917.

[20] Sack, P. J., & Lewis, L. L. (2012). Field-portable x-ray fluorescence spectrometer use in volcanogenic massive sulphide exploration with examples from the Touleary occurrence (MINFILE Occurrence 115O 176) in west-central Yukon. Yukon Geological Survey, Yukon Exploration and Geology, 115-131.

[21] Lacroix, E., Cauzid, J., Teitler, Y., & Cathelineau, M. (2021). Near real-time management

of spectral interferences with portable X-ray fluorescence spectrometers: application to Sc quantification in nickeliferous laterite ores. Geochemistry: Exploration, Environment, Analysis, 21(3), geochem2021-015.

[22] Purwadi, I., Casey, L. W., Ryan, C. G., Erskine, P. D., & van der Ent, A. (2022). X-ray fluorescence spectroscopy (XRF) for metallome analysis of herbarium specimens. Plant Methods, 18(1), 139.

[23] Durance, P., Jowitt, S. M., & Bush, K. (2014). An assessment of portable X-ray fluorescence spectroscopy in mineral exploration, Kurnalpi Terrane, Eastern Goldfields Superterrane, Western Australia. Applied Earth Science, 123(3), 150-163.

[24] Shalimba, E., Lohmeier, S., & Wanke, A. (2025). Application of portable X-ray fluorescence for exploration of carbonate-hosted sulfide mineralisation, Otavi Mountain Land, Namibia. International Science and Technology Journal of Namibia, 18(1), 1-24.

[25] Gray, C. A., & Van Rythoven, A. D. (2020). A comparative study of porphyry-type copper deposit mineralogies by portable X-ray fluorescence and optical petrography. Minerals, 10(5), 431.

[26] Liao, S., Tao, C., Li, H., Zhang, G., Liang, J., & Yang, W. (2017). Use of portable X-ray fluorescence in the analysis of surficial sediments in the exploration of hydrothermal vents on the Southwest Indian Ridge. Acta Oceanologica Sinica, 36(7), 66-76.

[27] Zhou, S., Yuan, Z., Cheng, Q., Weindorf, D. C., Zhang, Z., Yang, J., ... & Xie, S. (2020). Quantitative analysis of iron and silicon concentrations in iron ore concentrate using portable X-ray fluorescence (XRF). Applied Spectroscopy, 74(1), 55-62.

[28] Kowalska, S., Kubik, B., Skupio, R., & Wolański, K. (2020). Downhole lithological profile reconstruction based on chemical composition of core samples and drill cuttings measured with portable X-ray fluorescence spectrometer. Minerals, 10(12), 1101.